MOLEKUL
eISSN: 2503-0310

Articles
https://doi.org/10.20884/1.jm.2026.21.1.17186

Initial Screening of Heavy Metal Adsorption on Highly Porous Metal-Organic Frameworks based on MIL-101(Cr), Ethylenediamine-modified MIL-101(Cr), and MIL-101(Cr)-NH_2

Dendy Dendy[1], Witri Wahyu Lestari[1]*, Isa Anshori[2,3], Sentot Budi Rahardjo[1], Edi Pramono[1], Teguh Endah Saraswati[1], Fajar Rakhman Wibowo[1]

[1]Department of Chemistry, Faculty of Mathematics and Natural Sciences, Universitas Sebelas Maret, Surakarta, 57126, Indonesia
[2]Lab-on-Chip Group, Biomedical Engineering Department, Bandung Institute of Technology, Bandung, Indonesia
[3]Research Center for Nanosciences and Nanotechnology (RCNN) Bandung Institute of Technology, Bandung, Indonesia

*Corresponding author email: witri@mipa.uns.ac.id

Received October 02, 2025; **Accepted** February 16, 2026; **Available online** March 20, 2026

ABSTRACT. Heavy metal pollution is a significant environmental issue with detrimental effects on ecosystem and human health. Therefore, comprehensive handling need to be carried out. Herein we studied initial screening adsorption of heavy metals including Ni, Cu, Zn, Cd, and Pb using Metal-Organic Frameworks class of Materials Institute Lavoisier (MIL) based on Cr(III). MIL-101(Cr), and its modification with ethylenediamine (EA), and MIL-101(Cr)-NH_2 were prepared under hydrothermal condition. X-ray diffraction and FT-IR analysis confirmed the formation of the targeted materials. A new absorption band at 1050 cm^{-1} corresponds to vibration of C-N which indicates the successful EA modification into MIL-101(Cr). Nitrogen sorption isotherm measurement revealed MIL-101(Cr) and EA@MIL-101(Cr) have a specific surface area of 2548.6 and 2079 m^2/g with micropore-sized, while MIL-101(Cr)-NH_2 has a specific surface area of 1583.4 m^2/g with micro and mesopore-sized. Adsorption performance was assessed through batch experiments monitored by atomic absorption spectroscopy. The results show that MIL-101(Cr) and its modification with EA exhibit higher adsorption capacities on cadmium and nickel metal ions, compared to MIL-101(Cr)-NH_2. Meanwhile, MIL-101(Cr)-NH_2 and MIL-101(Cr) show more dominant adsorption capabilities on zinc and copper ions compared to the EA-modified MIL-101(Cr). This result suggests that the material's porosity still plays a dominant role in the adsorption processes compared to amine functionalize group on MIL itself.

Keywords: adsorption, chromium(III), heavy metals, MOF, MIL

INTRODUCTION

Heavy metal contaminations are a global environmental concern due to their non-degradability and toxicity to living organisms (Chen et al., 2020). Metal ions such as lead, cadmium, mercury, copper, chromium, zinc, nickel, and cobalt have detrimental effects on animals and the environment. Excessive consumption of heavy metals can lead to poisoning and negative impacts on organisms (Gouda & Taha, 2023). Soil heavy metal pollution is particularly concerning as it results in soil fertility degradation, reduced crop yield and quality, and poses a threat to human health (Wang et al., 2018; Zhu et al., 2019). Heavy metals can accumulate in the soil, water, and air, leading to long-term environmental contamination and potential harm to ecosystems (Gouda & Taha, 2023). Therefore, effective remediation strategies are necessary to mitigate the adverse effects of heavy metal pollution and protect the environment and human health (Wang et al., 2016).

Metal-organic frameworks (MOF) offer a new class of crystalline porous materials with fascinating structural topology and potential applications in various fields. As porous material, MOF show great potential for the adsorption and removal of metal ions, offering a promising approach for environmental remediation and analytical applications (Chen et al., 2020). MOF have emerged as promising materials for the adsorption of metal ions due to their large porosity and surface area. MOF have been used for the selective adsorption of heavy metal ions such as Pb(II) and Cu(II) (Elaiwi & Sirkecioglu, 2020; Lestari et al., 2023). The adsorption of these metal ions by MOF is rapid and efficient, making them suitable for preconcentration in water samples. The high surface areas of MOF and the presence of donor atoms make them suitable for the selective and sensitive preconcentration of trace amounts of heavy metal ions (Jamali et al., 2016).

MIL-101(Cr) is a well-studied chromium-based

metal-organic framework (MOF) that exhibits several superior properties and has a wide range of applications. It possesses an ultra-high specific surface area, large pore size, good thermal/chemical/water stability, and contains unsaturated Lewis acid (Cr^{3+}) sites in its structure (Chen et al., 2019; Shahriyari Far et al., 2021; Zou et al., 2022). The adsorption capacity and efficiency of MIL-101 have been investigated for various metal ions, including lead(II), cobalt(II), copper(II), and mercury(II) (Far et al., 2021; Lee & Choi, 2022; McElroy et al., 2020). Ethylenediamine-modified MIL-101(Cr) and MIL-101(Cr)-NH_2 are amine-functionalized versions of MIL-101(Cr) (Maponya et al., 2023; Vo et al., 2020). The introduction of amine functionality enhances the adsorption capacity of these MOF for the removal of Hg(II) in aqueous solution (Luo et al., 2016). The amine groups can be act as an active site that can coordinating with heavy metal ions, leading to improved adsorption performance (Elaiwi & Sirkecioglu, 2020; Luo et al., 2016).

Based on these considerations, MIL-101(Cr) was selected in this study because its chemical structure uniquely combines large pore accessibility, coordinatively unsaturated Cr^{3+} sites, and high structural stability under aqueous, acidic and basic conditions (Panda et al., 2020). The presence of large pores enables the rapid accommodation and diffusion of heavy metal ions with different ionic radii. At the same time, the Lewis acidic Cr^{3+} sites facilitate electrostatic interactions or coordination with metal ions (Zou et al., 2022). Moreover, the robust framework of MIL-101(Cr) allows post-synthesis modification (PSM) without significant loss of crystallinity, making it particularly suitable for evaluating the influence of surface functionalization on adsorption behavior. Dendy et al. (2025) has investigated the ratio of ethylendiamine (EA) functionalization in MIL-101(Cr) for indigo carmine adsorption and compared the performance with the pristine MIL-101(Cr) and MIL-101(Cr)-NH_2. Furthermore the family of these material,MIL-100(Cr) has also been composited with Indonesian natural zeolite for efficient CO_2 adsorption (Dendy et al. 2026)

The presence of appropriate porosity, surface area, and amine functional groups embedded in MIL-101(Cr)-NH_2 and ethylenediamine-modified MIL-101(Cr) is expected to enhance the adsorption capacity of this type of MOF toward heavy metal ions. However, despite numerous studies reporting enhanced adsorption after amine functionalization, a clear understanding of the relative contributions of textural properties and amine functional groups remains limited, particularly in the context of chromium-based MIL materials. Therefore, this study aims to conduct an initial screening and comparative evaluation of the adsorption behavior of MIL-101(Cr), ethylenediamine-modified MIL-101(Cr), and MIL-101(Cr)-NH_2 toward selected heavy metal ions, with a focus on identifying the influence of porosity, surface area, and amine functionalization in governing the adsorption process.

EXPERIMENTAL SECTION

Materials and Characterization

All reagents used in this research were Chromium(III) nitrate nonahydrate ($Cr(NO_3)_3{\cdot}9H_2O$, ≥ 99%), Terephthalic acid (H_2BDC, 98%), 2-amino terephthalic acid ($H_2BDC\text{-}NH_2$, 99%), ethylenediamine ($C_2H_8N_2$, ≥ 99%), N,N′-dimethylformamide (DMF, 99.8%), ethanol (96%), and n-hexane (95%) were purchased from Sigma Aldrich, Germany. Acetic acid glacial (CH_3COOH 100%), nitric acid (HNO_3 65%), chloroform ($CHCl_3$ ≥ 99%), and $Ni(NO_3)_2{\cdot}6H_2O$, $Cu(NO_3)_2{\cdot}3H_2O$, $Zn(NO_3)_2{\cdot}6H_2O$, $Cd(NO_3)_2.4H_2O$ solution 1000 ppm were commercially obtained from Merck, Germany. Distilled water was supplied by the CV Agung Jaya. The materials were used as purchased without any further purification.

X-ray diffractograms were obtained using Bruker D8 Advance Instrument (Germany) equipped with a Cu Kα incident beam (λ = 1.5418 Å) and a Ni filter. The operating parameters were fixed at 40 kV power, and data were collected in the 2θ range of 5–50°. Fourier transform infrared (FT-IR) spectra were acquired to identify the functional groups present in the materials, using a Shimadzu IR Prestige-21 spectrometer (Kyoto, Japan) with KBr pellets. The spectral range used was 400–4000 cm^{-1}, with 30 scans performed and a resolution of 2.0. The N_2 adsorption-desorption measurement were performed using Belsorp Mini X (USA) to calculate the specific surface area (BET method) and porosity (BJH method). The morphology, particle sizes, and elemental composition were analyzed using Field Emission Scanning Electron Microscopy-Energy Dispersive Spectroscopy (FESEM-EDS; JEOL JIB-4610F Multi Beam System, Japan). The thermal stability of materials were analyzed using TG/DTA (STA type, Linseis PT-1600, in the range temperature of 0-600 °C under nitrogen flow with heating rate 10 °C/min). Atomic absorption spectroscopy to measure the equilibrium concentration of a heavy metal solution using Shimadzu AA-6650 (Kyoto, Japan).

Synthesis of MIL-101(Cr) and MIL-101(Cr)-NH_2

Synthesis of MIL-101(Cr) was carried out hydrothermally according to Zhao et al. (2018). In beaker A, $Cr(NO_3)_3{\cdot}9H_2O$ (6 g) was dissolved in 32.75 mL of distilled water. Another beaker (B) was prepared and filled with 2.5 g of H_2BDC dissolved in 32.75 mL of distilled water. Each beaker was swirled for 15 minutes at room temperature. Following that, the solution in beaker B was progressively poured into beaker A and stirred for 15 minutes. After adding 2.33 M acetic acid (10 mL), the solution was agitated for another 15 minutes. The solution was then placed in Teflon and autoclaved for 20 hours at 220 °C. The precipitate was then washed twice with 25 mL of DMF and ethanol. The washed solid was immersed in

chloroform for three days to allow for solvent exchange. The solid was then dried and activated for 2 hours in a 120 °C oven.

Synthesis of MIL-101(Cr)-NH_2 was also conducted hydrothermally referring to Vo et al. (2020). In beaker A, $Cr(NO_3)_3{\cdot}9H_2O$ (1.6 g) was dissolved in 12.5 mL of distilled water. In another beaker (B), dissolved 0.72 g of the ligand H_2BDC-NH_2 in 12.5 mL of distilled water. At room temperature, each beaker was stirred for 15 minutes. The solution in beaker B was then slowly poured into beaker A and agitated for another 15 minutes. The mixture was then sonicated for 10 minutes before being placed in Teflon and autoclaved for 24 hours at 150 °C. The resulting solid was then washed twice with 25 mL of DMF and ethanol at 70 °C, each. The solid was then dried and activated in an oven at 80 °C for 12 hours.

Modification of MIL-101(Cr) with EA via Post-Synthesis Approach

MIL-101(Cr) was modified with EA via PSM, as described by Zhong et al. (2018). A total of 0.5 grams of synthesized MIL-101(Cr) was activated by heating at 150 °C for 10 hours. MIL-101(Cr) activation was then dissolved in 50 mL n-hexane and sonicated for 20 minutes. The suspension was then slowly mixed in with 0.2 mL EA and stirred at room temperature for 30 minutes. The mixture was covered and left for 4 hours before being dried at room temperature and activated for 5 hours at 150 °C.

Initial Screening of Heavy Metal Adsorption

The batch approach was used for the initial screening of heavy metal adsorption. Amounts of 20 mg of MIL-101(Cr), its modification (EA@MIL-101), and MIL-101(Cr)-NH_2 were placed in an Erlenmeyer flask containing 20 mL of Ni(II), Cu(II), Zn(II), Pb(II), and Cd(II) solution 50 ppm as the initial concentration (C_o). Then, shake the mixture at 140 rpm for 6 hours. The mixture was filtered using Whatman paper when it reached equilibrium. AAS spectrometry was used to estimate the equilibrium concentration of heavy metal ions (C_e) in the filtrate. The amount of heavy metal ions adsorbed can be calculated using equation (1), which calculates the difference between the initial and equilibrium concentrations of heavy metal ions in solution (Wu et al., 2019).

$$\%\ Adsorption\ = \frac{C_o - C_e}{C_o} x\ 100\% \qquad (1)$$

Where V is the volume of the heavy metal solution (mL), C_o is the initial concentration of the heavy metal solution (ppm), and C_e: the equilibrium concentration of the heavy metal solution (ppm).

RESULTS AND DISCUSSION

Material Characterization

XRD characterization demonstrated the effective synthesis of MIL-101(Cr), EA@MIL-101(Cr), and MIL-101(Cr)-NH_2 as reported previously (Dendy et al. 2025). The diffractogram of the synthesized findings compared to the CCDC MIL-101 standard (No. 605510) is shown in **Figure 1**. Based on the diffractogram, MIL-101(Cr) and MIL-101(Cr)-NH_2 have diffraction patterns that meet the standard by Lebedev et al. (2005). MIL-101(Cr) and MIL-101(Cr)-NH_2 share the typical MIL-101 standard peaks at 2θ 8.4°, 8.9°, 10.2°, and 16.4°, demonstrating the success of the synthesis. When the MIL-101(Cr)-NH_2 diffractogram was compared to the standard, a widened peak at 8.9° was observed. According to Han et al. (2020), the broadening peak of the MIL-101(Cr)-NH_2 diffractogram was produced by the very small crystallite size, based on the Scherer equation. The diffraction pattern of EA@MIL-101(Cr) demonstrates that the addition of EA has no effect on MIL-101(Cr) characteristic peaks. The intensity of the typical 2θ peaks unaffected after attaching EA, indicating that the structure of MIL-101(Cr) has remains and not changed. This demonstrates the effectiveness of the EA adjustments into MIL-101(Cr).

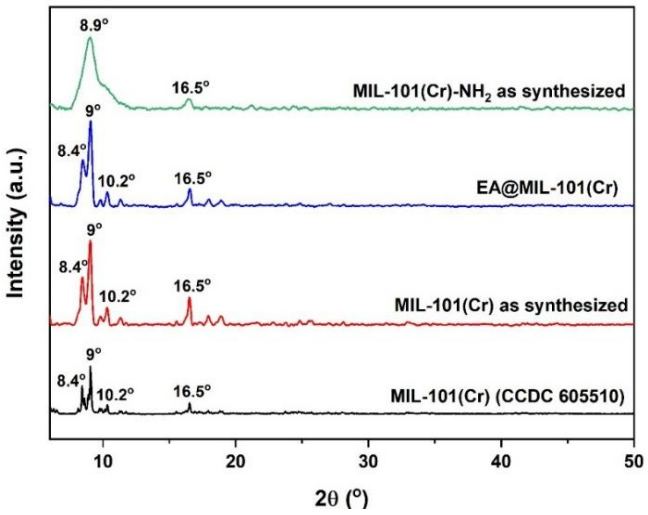

Figure 1. X-ray diffractogram of synthesized MIL-101(Cr) (red), EA@MIL-101(Cr) (blue), and MIL-101(Cr)-NH_2 (green)

To further understand. the peak broadening observed in the XRD patterns, the full width at half maximum (FWHM) values of the characteristic peaks of the materials were extracted and summarized in **Table 1**. MIL-101(Cr) exhibits relatively narrow diffraction peaks, with FWHM values ranging from 0.23° to 0.36°, corresponding to an average crystallite size of 29.95 nm estimated using the Scherrer equation. A comparable peak sharpness is observed for EA@MIL-101(Cr). The FWHM values are slightly higher (0.26–0.44°). The average crystallite size is 26.53 nm, indicating that ethylenediamine modification via a post-synthesis approach does not decline the crystallinity of the MIL-101(Cr) framework (Dendy et al., 2025). In contrast, MIL-101(Cr)-NH_2 shows substantially broader diffraction peaks, particularly at $2\theta \approx 8.9°$ and 16.5°, with FWHM values of 1.62° and 0.91°, respectively. This pronounced peak broadening corresponds to a markedly smaller average crystallite size of 7.21 nm. The small crystallite size suggests either limited crystal growth or increased lattice distortion during synthesis, which is consistent with the lower synthesis temperature and the presence of amine-functionalized linkers (Jannat et al., 2025; Mourdikoudis et al., 2018). It should be noted that the crystallite size derived from XRD reflects the coherent diffraction domain rather than the particle size observed by SEM. Therefore, the nanoscale particles of MIL-101(Cr)-NH_2 are likely polycrystalline in nature and may also exhibit higher microstrain, both of which contribute to the observed peak broadening. Overall, the FWHM and Scherrer analyses provide evidence of the crystallinity differences among the synthesized materials.

The functional groups of MIL-101(Cr), EA@MIL-101(Cr), and MIL-101(Cr)-NH_2 were analyzed using FT-IR to confirm the success of their synthesis. Figure 2a shows the spectra of MIL-101(Cr) having functional group absorption bands originating from the H_2BDC ligand (Pourebrahimi et al., 2017), such as at 1595 and 1393 cm^{-1} (asymmetric and symmetric vibrations of the O-C-O group), 750 cm^{-1} (vibration of the C-H group comes from the benzene ring), and at 1657 cm^{-1} (vibration of the C=O group) which has a shift from 1688 cm^{-1} in the H_2BDC ligand spectra. The shift suggests ligand deprotonation occurred and then coordinate with the central metal ion, as evidenced by the emergence of a new Cr-O coordination bond absorption band at 575 cm^{-1} (Chen et al., 2019). A broad peak corresponding to the O-H functional group vibration, arising from water molecules emerges in the absorption band 3500-3081 cm^{-1}. The O-H group peak is wider compared to the H_2BDC ligand spectra, indicating the production of interactions between water molecules and Cr^{3+} ions in MIL-101(Cr) (Shadmehr et al., 2019). **Figure 2a** further indicates that the FT-IR spectra of EA@MIL-101(Cr) matches the spectrum of MIL-101(Cr) prior to alteration. The appearance of new absorption bands at 1050 cm^{-1} (C-N group vibration), 3242 and 3139 cm^{-1} (N-H group vibration), and 2955 and 2894 cm^{-1} (Aliphatic C-H group vibration) that reveal the success of the modification (Asghar et al., 2020; Zhong et al., 2018). Furthermore, wavenumbers 1612 and 1391 cm^{-1} show the existence of EA (vibration of the Cr-N group) which is overlap with the vibration of the O-C-O group of the carboxylate linker (Budiasih et al., 2013). Therefore, the absorption relative tends to broadens compared to the spectra before modification.

The FT-IR spectra of MIL-101(Cr)-NH_2 and its ligand H_2BDC-NH_2 are shown in **Figure 2b**. The existence of an absorption band from the ligand functional group in the MIL-101(Cr)-NH_2 spectra indicates that the synthesis was successful. Wavenumbers at 3490 and 3363 cm^{-1} (N-H group vibration), 1498 and 1432 cm^{-1} (asymmetric and symmetric O-C-O group vibration), 1340 and 1259 cm^{-1} (C-N group of the benzene ring vibration), and a shift in vibrational C=O group at wavenumbers 1657 and 1688 cm^{-1} caused by coordination of the ligand and central metal ion as previously explained (Luo et al., 2016). A new absorption observed at 540 cm^{-1}, which alludes to the establishment of Cr-O bond coordination, further supports this coordination (Tian et al., 2016).

The typical FTIR bands and their intensities are summarized in **Table 2** to clarify the chemical functional groups present in each material. All samples display typical bands associated with the MIL-101 framework, including coordinated carboxylate groups (C=O and O–C–O vibrations) and Cr–O bonds. This confirms the preservation of the framework structure after modification. Furthermore, the presence of N–H and C–N stretching bands in EA@MIL-101(Cr) and MIL-101(Cr)-NH_2 indicates the successful introduction of amine functionalities.

These functional groups play a distinct role in heavy metal adsorption. Unsaturated Cr^{3+} sites offer Lewis acidic and electrostatic interaction sites for metal ions, while amine groups can serve as electron-donating ligands that enhance chelation with metal ions that have high complexation constants, such as

Table 1. FWHM values and crystallite size of MIL-101(Cr), EA@MIL-101(Cr), and MIL-101(Cr)-NH_2

Materials	FWHM value at 2θ (°)				Average Crystallite Size (nm)
	~8.4	~8.9	~10.2	~16.5	
MIL-101(Cr)	0.36	0.31	0.25	0.23	29.95
EA@MIL-101(Cr)	0.44	0.35	0.26	0.27	26.53
MIL-101(Cr)-NH_2	-	1.62	-	0.91	7.21

Cu^{2+} and Zn^{2+} (Sharifzadeh et al., 2025). However, the adsorption results indicate that having amine groups alone does not ensure better adsorption performance. Instead, the adsorption behavior is influenced by the combined effects of the availability of functional groups and the material's textural properties, particularly its surface area and pore accessibility (Ogunedo et al., 2025). This explains the reason MIL-101(Cr)-NH_2 shows improved adsorption for certain metal ions despite having a lower surface area, whereas MIL-101(Cr) and EA@MIL-101(Cr) demonstrate better performance for ions that rely on pore-filling for adsorption.

The morphology, average particle size distribution, and elemental content of MIL-101(Cr), EA@MIL-101(Cr), and MIL-101(Cr)-NH_2 were disclosed by FESEM-EDS analysis. MIL-101(Cr) and EA@MIL-101(Cr) have octahedron morphologies, as exposed in **Figure 3**, whereas MIL-101(Cr)-NH_2 has aggregated spheroid nanoparticle. According to several references, the morphology of MIL-101(Cr) and MIL-101(Cr)-NH_2 is an octahedron and aggregated spheroid, respectively (Alivand et al., 2019; Vo et al., 2020). As a result, the morphology of the synthesized MOF is appropriate, and the synthesis was successful. **Figure 3** depicts the average particle size distribution graph of the three MOFs, which are 301.38 ± 62.35 nm (MIL-101(Cr)); 301.75 ± 58.94 nm (EA@MIL-101(Cr)); and 33.26 ± 7.72 nm (MIL-101(Cr)-NH_2). Based on the result, the addition of EA via PSM approach has no effect on particle size distribution. The lack of observed particle size change is most likely due to EA adhering to the pores of the MOF. The particle size distribution of MIL-101(Cr)-NH_2 is nanoscale, which agrees with the broadening of 2θ peak on the MIL-101(Cr)-NH_2 diffractogram. **Table 3** shows the elemental compositions of MIL-101(Cr), EA@MIL-101(Cr), and MIL-101(Cr)-NH_2. After introducing EA, the percentages of Cr, C, and O atoms changed. The addition of EA at unsaturated metal sites reduced the percentage of Cr atoms, while the replacement of water molecules by EA reduced the number of O atoms. The rise in C atoms after modification is attributed to the increase in C atoms from EA in MOF (Zhang et al., 2015). This percentage change demonstrates the success of the modification.

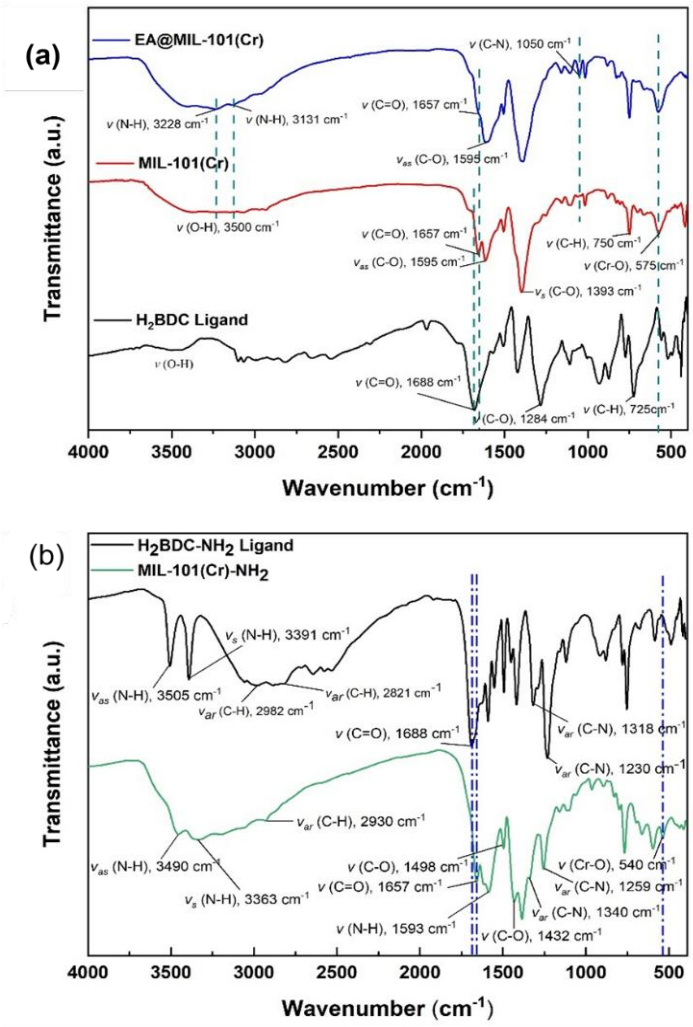

Figure 2. FTIR spectra of (**a**) MIL-101(Cr) (red) compared to H_2BDC and EA@MIL-101(Cr) (blue) and (**b**) MIL-101(Cr)-NH_2 (green) compared to H_2BDC-NH_2

Table 2. FTIR characteristic bands of MIL-101(Cr), EA@MIL-101(Cr), and MIL-101(Cr)-NH_2

Absorption of functional groups	MIL-101(Cr)		EA@MIL-101(Cr)		MIL-101(Cr)-NH_2	
	Wavenumber (cm^{-1})	Intensity	Wavenumber (cm^{-1})	Intensity	Wavenumber (cm^{-1})	Intensity
O–H stretching	3500–3081	strong	3500–3081	strong	3500–3080	strong
N–H stretching	-	-	3242, 3139	medium	3490, 3363	medium
C=O stretching (coordinated carboxylate)	1657	strong	1657	strong	1657	strong
Asymmetric O–C–O stretching	1595	strong	1595, 1393	strong	1498	strong
Symmetric O–C–O stretching	1393	strong	1393	strong	1432	strong
C–N stretching	-	-	1050	weak	1340, 1259	strong
Cr–O vibration	575	strong	575	strong	540	strong

Table 3. Elemental content of MIL-101(Cr), EA@MIL-101(Cr), and MIL-101(Cr)-NH_2 observed by EDS analysis

Materials	Elemental Content (%Atom)			
	C	O	Cr	N
MIL-101(Cr)	71.6	25.6	2.8	-
EA@MIL-101(Cr)	75.6	22.3	2.1	Not detected
MIL-101(Cr)-NH_2	73	21.1	5.9	Not detected

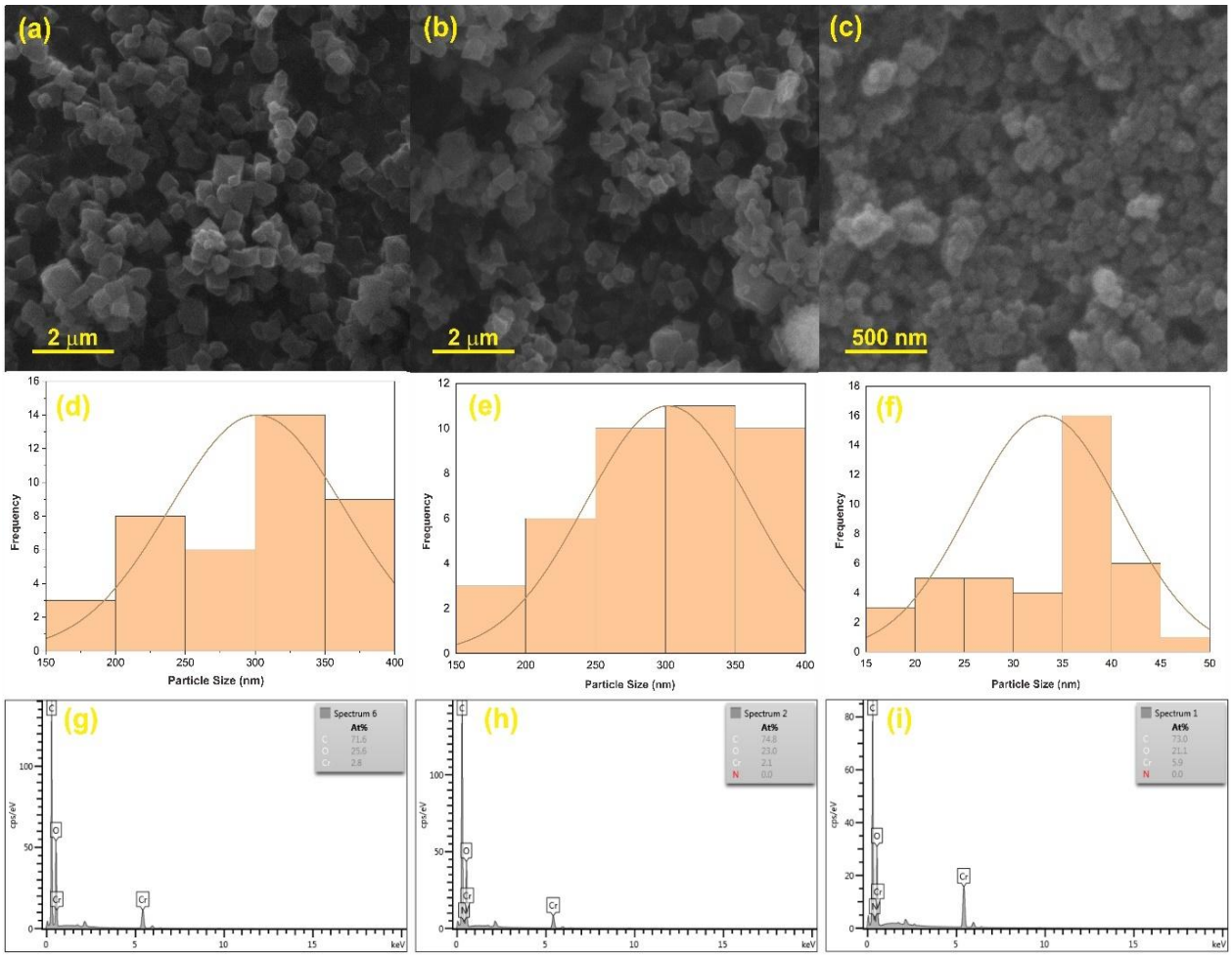

Figure 3. SEM images of MIL-101(Cr) (**a**); EA@MIL-101(Cr) (**b**); MIL-101(Cr)-NH_2 (**c**), average particle size distribution graph of MIL-101(Cr) (**d**); EA@MIL-101(Cr) (**e**); MIL-101(Cr)-NH_2 (**f**), EDS spectra of MIL-101(Cr) (**g**); EA@MIL-101(Cr) (**h**); MIL-101(Cr)-NH_2 (**i**)

The thermal stability of MIL-101(Cr), EA@MIL-101(Cr), and MIL-101(Cr)-NH_2 were determined by TGA characterization. According to the findings of the measurements, the mass loss in MIL-101(Cr), EA@MIL-101(Cr), and MIL-101(Cr)-NH_2 ensued in three stages (as shown in **Figure 4**), as reported by Liu et al. (2017), Shadmehr et al. (2019), and Luo et al. (2016). The first stage mass loss for MIL-101(Cr) and EA@MIL-101(Cr) was 11.21% and 8.52%, respectively, occurred at 28-100 °C. Based on calculations, the mass loss is expected to be evaporation of 5 and 4 water molecules which trapped in the pores of MIL-101(Cr) and EA@MIL-101(Cr), respectively. For the first stage of mass loss, MIL-101(Cr)-NH_2 occurred at 28-150 °C with a mass loss of 35.34%, which was calculated to be released 5 molecules of water and ethanol solvent. The second stage of mass loss observed at the temperature range 100-300 °C for MIL-101(Cr) and EA@MIL-101(Cr), with 12.85% and 14.29% of the mass loss. This stage was related to the elimination of 4 water molecules which coordinated to the Cr^{3+} sites (MIL-101(Cr)) and 1 hydroxyl molecule and 2 EA molecules for EA@MIL-101(Cr). In this range, the mass loss of EA@MIL-101(Cr) is slightly larger due to one of the released molecules is almost certainly EA, which has a higher relative atomic mass than water. The second stage of mass loss in MIL-101(Cr)-NH_2 is likely caused by the released of water molecules coordinated with the chromium saturated sites, as described previously. This mass loss observed at 150-300 °C, with a loss of 16.31%, is attributed to elimination of 8 water molecules. The final mass loss for MIL-101(Cr), EA@MIL-101(Cr), and MIL-101(Cr)-NH_2 which observed above 300 °C, by 36.78%; 38.13%; and 23.43%, respectively. The decrease related to the organic decomposition of BDC_2- ligand (MIL-101(Cr) and its modification) and NH_2-BDC_2^- ligand (MIL-101(Cr)-NH_2) which caused degradation to the MOF frameworks. Hence, the three MOFs have thermal stability up to 300 °C analogous as reported by Liu et al. (2017), Shadmehr et al. (2019), and Luo et al. (2016).

The lower apparent thermal stability of MIL-101(Cr)-NH_2 compared to MIL-101(Cr) can be primarily attributed to differences in guest molecule retention and surface chemistry. As observed from the TGA profiles, MIL-101(Cr)-NH_2 exhibits a significantly higher mass loss at the initial stage (28–150 °C), which is associated with the release of a larger amount of physically adsorbed water and residual solvent molecules. This behavior indicates a more hydrophilic character of MIL-101(Cr)-NH_2, arising from the presence of amine functional groups that can form hydrogen-bonding interactions with polar molecules, thereby increasing solvent retention within the pores.

In addition, the introduction of –NH_2 groups alters the local chemical environment of the framework, potentially reducing the overall rigidity of the coordination network under thermal stress. The amine-functionalized linker can induce local structural distortion and enhanced lattice flexibility, making the framework more susceptible to thermal perturbation. Consequently, although the main framework decomposition of MIL-101(Cr)-NH_2 still occurs at comparable temperatures to MIL-101(Cr), the higher mass loss at lower temperatures suggests reduced thermal stability. These results suggest that the observed difference in thermal behavior is mainly related to enhanced guest–framework interactions and increased framework flexibility induced by amine functionalization, rather than premature collapse of the MIL-101 structure.

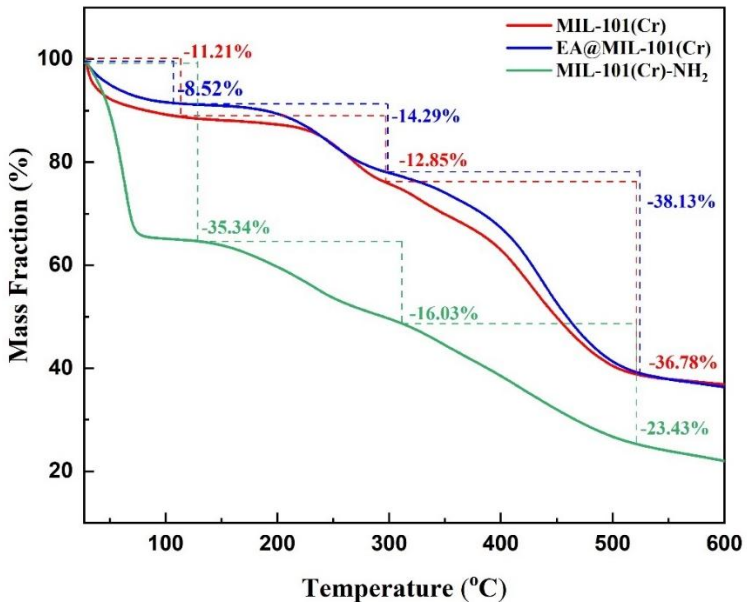

Figure 4. Thermogram of MIL-101(Cr) (red), EA@MIL-101(Cr) (blue), and MIL-101(Cr)-NH_2 (green)

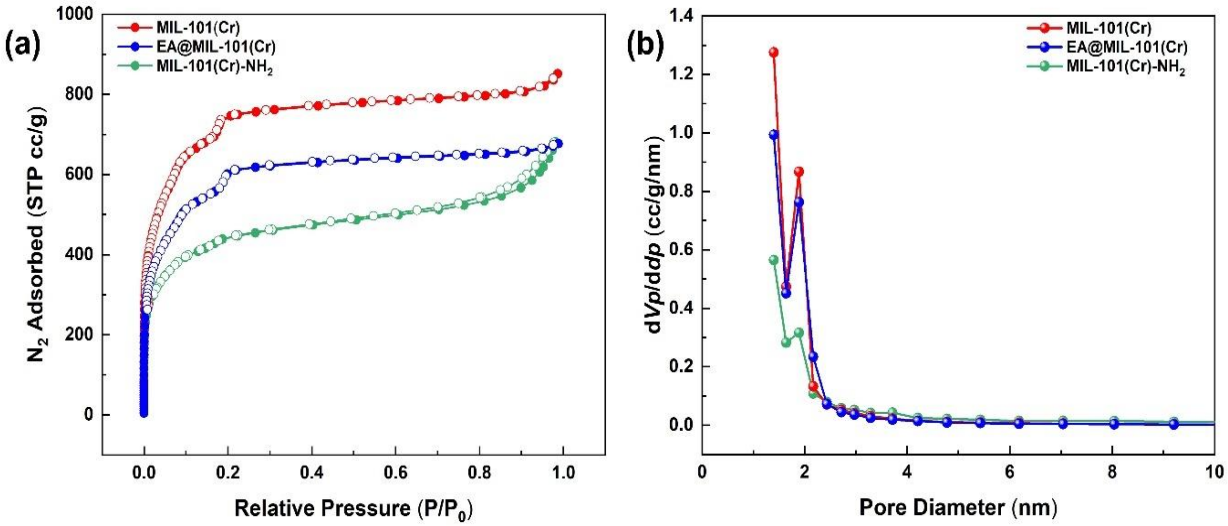

Figure 5. (**a**) Nitrogen adsorption-desorption isotherm and (**b**) pore size distribution graph of of MIL-101(Cr) (red); EA@MIL-101(Cr) (blue); MIL-101(Cr)-NH_2 (green)

Nitrogen adsorption-desorption measurements were used to determine the specific surface area and porosity of MIL-101(Cr), EA@MIL-101(Cr), and MIL-101(Cr)-NH_2. The results of measurements utilizing the Brunauer-Emmett-Teller (BET) and Barrett-Joyner-Halenda (BJH) methods revealed that the incorporating EA reduces specific surface area and porosity. This drop demonstrates the effectiveness of adding EA to MIL-101(Cr). Before and after the addition of EA, the specific surface area was 2548.6 m^2/g and 2079 m^2/g, respectively. MIL-101(Cr) porosity, including pore volume and diameter, of 0.9548 cm^3/g and 1.8811 nm. Meanwhile, EA@MIL-101(Cr) has pore volume and diameter of 0.7989 cm^3/g and 1.8236 nm. All of these reductions also explain that EA incorporated within the pores of MIL-101(Cr) (Zhong et al., 2018). According to **Figure 5a**, the type of adsorption-desorption isotherm for all materials followed type I, which denotes as microporous material (Trung et al., 2010). As shown in the pore size distribution graph (**Figure 5b**), this pore type is appropriate for MIL-101(Cr) and EA@MIL-101(Cr). Meanwhile, MIL-101(Cr)-NH_2 has classified mesoporous based on the pore size, 2.9896 nm. The distribution graph clarifies this disparity since the MIL-101(Cr)-NH_2 exhibits non-uniformly pore diameter, which is dominated by mesopores (Jiang et al., 2012). The specific surface area and pore volume of MIL-101(Cr)-NH_2 were 1583.4 m^2/g and 0.7769 cm^3/g, respectively. The textural properties of MIL-101(Cr), EA@MIL-101(Cr), and MIL-101(Cr)-NH_2 are consistent with previous report (Han et al., 2020; Vo et al., 2020; Zhao et al., 2018; Zhong et al., 2018).

Initial Screening of Heavy Metal Adsorption

The initial screening of heavy metal adsorption was conducted to determine the factors affecting the adsorption performance of the three MOF towards each type of heavy metal ion. The influential factors including porosity, specific surface area, and functional groups will be investigated here. As we know, each heavy metal ion has different characteristics for example ion size or radius, electronegativity, complexation constant, and solubility under certain pH conditions (Elaiwi & Sirkecioglu, 2020; Guo et al., 2014; Luo et al., 2015). Therefore, understanding the factors that affect the adsorption performance of the three MOF becomes an important key while forecasting the processes or interactions that occur. At this initial screening stage, all heavy metal solutions were prepared in the same way without further adjusting pH. **Figure 6** reveals the results of heavy metal adsorption using the three MOF. The results exhibited some certain trends. MIL-101(Cr) and EA@MIL-101(Cr) tend to have large percent adsorption on Cd^{2+} and Ni^{2+}. In contrast, the adsorption performance of MIL-101(Cr) and MIL-101(Cr)-NH_2 tends to be more favorable on Zn^{2+} and Cu^{2+}. The removal of Cd^{2+} and Ni^{2+} is greater on MIL-101(Cr) and EA@MIL-101(Cr) due to the large ionic radius of Cd^{2+} (0.95 Å). The specific surface area and pore volume of these both MOFs are larger compared to MIL-101(Cr)-NH_2 allowing the adsorption process to be maximized (Luo et al., 2015). Slightly different from Cd^{2+}, Ni^{2+} has a small ionic radius (0.7 Å) which makes the pore diameter of the material is going to be crucial (Mobasherpour et al., 2012). MIL-101(Cr) and EA@MIL-101(Cr) have micropores that enable the Ni^{2+} adsorption process to be more selective and preferable. In fact, the large adsorption of Ni^{2+} is also influenced by the electronegativity (1.91) and the large complexation constant (18.62) which leads to the coordination of chelate between Ni and amine on EA@MIL-101(Cr) (Luo et al., 2015).

The adsorption on MIL-101(Cr)-NH_2 was dominant to Cu^{2+} similar to Elaiwi & Sirkecioglu (2020). This is attributed to the highest complexation constant of Cu^{2+} (1.9) among all the heavy metals tested. The amine groups on MIL-101(Cr)-NH_2 are more abundant rather

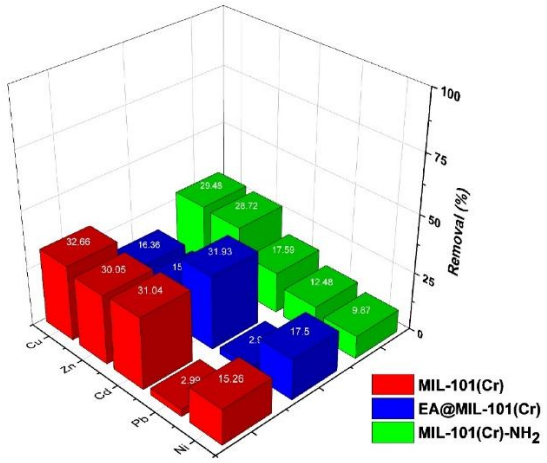

Figure 6. Percent removal of MIL-101(Cr) (red); EA@MIL-101(Cr) (blue); MIL-101(Cr)-NH_2 (green)

than EA@MIL-101(Cr) due to its own ligand thus assisting the formation of chelates as interactions during the adsorption process (Luo et al., 2016). In this case, the functional groups plays a greater role than porosity or specific surface area. On the other hand, in the case of Zn^{2+}, the adsorption of MIL-101(Cr)-NH_2 is more significant due to its functional groups and porosity. The complexity constant of Zn^{2+} is considerable (16.5) and its ionic radius is less when compared to Cd^{2+} (Mekatel et al., 2012). The presence of amine groups and a large specific surface area led the adsorption percentage to be comparable to MIL-101(Cr), which has a greater surface area and porosity. In general, the adsorption performance of these heavy metals depends on the specific surface area and porosity of the adsorbent material. It can be observed that MIL-101(Cr) almost dominates in some instances. Although it is possible that functional group factors also play a role. Therefore, the most possible mechanism for the initial screening process of heavy metal adsorption is pore-filling (Rego et al., 2021).

Overall, the observed removal efficiencies can be rationalized by integrating the structural, textural, and chemical characteristics of the synthesized materials. Although amine functionalization introduces additional coordination sites, the adsorption performance in this study is primarily governed by surface area, pore accessibility, and framework integrity. The parent MIL-101(Cr) exhibits the highest specific surface area and well-defined micropores, which collectively facilitate efficient diffusion and pore-filling-dominated adsorption of heavy metal ions. In contrast, the EA modification partially occupies the pore space, whereas MIL-101(Cr)-NH_2 exhibits a significant reduction in surface area, limiting the number of accessible adsorption sites despite the presence of amine groups. As a result, MIL-101(Cr)-NH_2 displays selective enhancement toward metal ions with high complexation tendencies (Cu^{2+} and Zn^{2+}). In contrast, the parent MIL-101(Cr) achieves superior overall removal efficiency due to its optimal balance between porosity, accessibility, and structural robustness. These findings highlight that surface functionalization does not necessarily guarantee improved adsorption performance when it compromises the intrinsic textural advantages of the parent MOF.

CONCLUSIONS

Highly porous MOFs based on MIL-101(Cr), amine-modified MIL-101(Cr), and MIL-101(Cr)-NH2 have been successfully synthesized and applied in initial screening of heavy metal adsorption. The adsorption results demonstrated that some MOFs have a tendency to adsorb specific types of heavy metals depending on their characteristics. Based on the adsorption results, it is suggested that specific surface area and porosity are the major factors influencing the adsorption of these various heavy metal ions. Another influential factor is the presence amine group which contributed in the chelate formation within the heavy metal ion so that interactions can occurred during the adsorption process. The best adsorption results of heavy metal ions using MIL-101(Cr) and EA@MIL-101(Cr) were Cd^{2+} by 31.04 & 31.09% respectively and Ni^{2+} by 17.5 & 15.26% when compared to MIL-101(Cr)-NH_2. During the removal process, specific surface area and porosity are the important factors involved during the adsorption process. However, MIL-101(Cr)-NH_2 has the highest percent adsorption on Cu^{2+} and Zn^{2+} adsorption of 29.48 and 28.72% when compared to EA@MIL-101(Cr). These results are influenced by the role of functional groups and specific surface area during the adsorption process. These results provide an insight that incorporating functional groups into a material does not always result the outstanding adsorption capabilities. The textural properties of the material must also be considered.

ACKNOWLEDGEMENTS

We would like to acknowledge Universitas Sebelas Maret (UNS) for providing research funding under PNBP research grant via the scheme Mandatory research grant project number 228/UN27.22/PT.01.03/2023.

REFERENCES

Asghar, A., Iqbal, N., Aftab, L., Noor, T., Kariuki, B. M., Kidwell, L., & Easun, T. L. (2020). Ethylenediamine loading into a manganese-based metal-organic framework enhances water stability and carbon dioxide uptake of the framework. *Royal Society Open Science*, *7*(3). https://doi.org/10.1098/rsos.191934

Bobbitt, N. S., Mendonca, M. L., Howarth, A. J., Islamoglu, T., Hupp, J. T., Farha, O. K., & Snurr, R. Q. (2017). Metal-organic frameworks for the removal of toxic industrial chemicals and chemical warfare agents. *Chemical Society Reviews*, *46*(11), 3357–3385. https://doi.org/10.1039/c7cs00108h

Budiasih, K. S., Anwar, C., Santosa, S. J., & Ismail, H. (2013). Synthesis and Characterization of chromium (III) complexes with L-glutamic acid, glycine and L- cysteine. *World Academy of Science, Engineering and Technology*, *78*(Iii), 1927–1931.

Carson, F., Su, J., Platero-Prats, A. E., Wan, W., Yun, Y., Samain, L., & Zou, X. (2013). Framework isomerism in vanadium metal-organic frameworks: MIL-88B(V) and MIL-101(V). *Crystal Growth and Design*, *13*(11), 5036–5044. https://doi.org/10.1021/cg4012058

Chen, M. L., Zhou, S. Y., Xu, Z., Ding, L., & Cheng, Y. H. (2019). Metal-organic frameworks of MIL-100(Fe, Cr) and MIL-101(Cr) for aromatic amines adsorption from aqueous solutions. *Molecules*, *24*(20). https://doi.org/10.3390/molecules24203718

Chen, X., Chen, D., Li, N., Xu, Q., Li, H., He, J., & Lu, J. (2020). Modified-MOF-808-loaded polyacrylonitrile membrane for highly efficient, simultaneous emulsion separation and heavy metal ion removal. *ACS Applied Materials and Interfaces*, *12*(35), 39227–39235. https://doi.org/10.1021/acsami.0c10290

Chen, Y., Bai, X., & Ye, Z. (2020). Recent progress in heavy metal ion decontamination based on metal–organic frameworks. *Nanomaterials*, *10*(8), 1–23. https://doi.org/10.3390/nano10081481

Elaiwi, F. A., & Sirkecioglu, A. (2020). Amine-functionalized metal organic frameworks MIL-101(Cr) adsorbent for copper and cadmium ions in single and binary solution. *Separation Science and Technology (Philadelphia)*, *55*(18), 3362–3374. https://doi.org/10.1080/01496395.2019.1706571

Gouda, S. A., & Taha, A. (2023). Biosorption of heavy metals as a new alternative method for wastewater treatment: A Review. *Egyptian Journal of Aquatic Biology and Fisheries*, *27*(2), 135–153. https://doi.org/10.21608/ejabf.2023.291671

Guo, X., Du, B., Wei, Q., Yang, J., Hu, L., Yan, L., & Xu, W. (2014). Synthesis of amino functionalized magnetic graphenes composite material and its application to remove Cr(VI), Pb(II), Hg(II), Cd(II) and Ni(II) from contaminated water. *Journal of Hazardous Materials*, *278*, 211–220. https://doi.org/10.1016/j.jhazmat.2014.05.075

Han, G., Qian, Q., Mizrahi Rodriguez, K., & Smith, Z. P. (2020). Hydrothermal synthesis of sub-20 nm amine-functionalized MIL-101(Cr) nanoparticles with high surface area and enhanced CO_2 uptake. *Industrial and Engineering Chemistry Research*, *59*(16), 7888–7900. https://doi.org/10.1021/acs.iecr.0c00535

Jamali, A., Tehrani, A. A., Shemirani, F., & Morsali, A. (2016). Lanthanide metal-organic frameworks as selective microporous materials for adsorption of heavy metal ions. *Dalton Transactions*, *45*(22), 9193–9200. https://doi.org/10.1039/c6dt00782a

Jiang, D., Keenan, L. L., Burrows, A. D., & Edler, K. J. (2012). Synthesis and post-synthetic modification of MIL-101(Cr)-NH_2 via a tandem diazotisation process. *Chemical Communications*, *48*(99), 12053–12055. https://doi.org/10.1039/c2cc36344e

Kalhor, S., Zarei, M., Zolfigol, M. A., Sepehrmansourie, H., Nematollahi, D., Alizadeh, S., Shi, H., & Arjomandi, J. (2021). Anodic electrosynthesis of MIL-53(Al)-$N(CH_2PO_3H_2)_2$ as a mesoporous catalyst for synthesis of novel (N-methyl-pyrrol)-pyrazolo[3,4-b]pyridines via a cooperative vinylogous anomeric based oxidation. *Scientific Reports*, *11*(1), 1–20. https://doi.org/10.1038/s41598-021-97801-7

Lebedev, O. I., Millange, F., Serre, C., Van Tendeloo, G., & Férey, G. (2005). First direct imaging of giant pores of the metal-organic framework MIL-101. *Chemistry of Materials*, *17*(26), 6525–6527. https://doi.org/10.1021/cm 051870o

Lee, J. Y., & Choi, J.-H. (2022). Copper-based metal-organic framework for highly efficient adsorption of lead ions from aqueous solution. *Materials Research Express*, *9*(9), 95505. https://doi.org/10.1088/2053-1591/ac93ea

Lestari, W. W., Meilani, R., Nurcahyo, I. F., Larasati, L., & Dendy, D. (2023). In Situ Electro-synthesis of EDTA-Modified MIL-100(Fe) as an enhanced candidate detoxifying agent for pb(ii) and its adsorption characteristics. *Journal of Inorganic and Organometallic Polymers and Materials*. https://doi.org/10.1007/s10904-023-02868-6

Liu, L., Tai, X., & Zhou, X. (2017). Au^{3+}/Au^0 supported on chromium(III) terephthalate metal organic framework (MIL-101) as an efficient heterogeneous catalystfor three-component coupling synthesis of propargylamines.

Materials, *10*(2). https://doi.org/10.3390/ma10020099

Luo, X., Ding, L., & Luo, J. (2015). Adsorptive removal of Pb(II) ions from aqueous samples with amino-functionalization of metal-organic frameworks MIL-101(Cr). *Journal of Chemical and Engineering Data*, *60*(6), 1732–1743. https://doi.org/10.1021/je501115m

Luo, X., Shen, T., Ding, L., Zhong, W., Luo, J., & Luo, S. (2016). Novel thymine-functionalized MIL-101 prepared by post-synthesis and enhanced removal of Hg^{2+} from water. *Journal of Hazardous Materials*, *306*, 313–322. https://doi.org/10.1016/j.jhazmat.2015.12.034

Maponya, T., Makgopa, K., Somo, T. R., Tshwane, D. M., & Modibane, K. D. (2023). Ethylenediamine functionalized waste polyethylene terephthalate-derived metal-organic framework for adsorption of palladium ions from aqueous solutions. *Cleaner Chemical Engineering*, *6*, 100106. https://doi.org/https://doi.org/10.1016/j.clce.2023.100106

Mekatel, H., Amokrane, S., Benturki, A., & Nibou, D. (2012). Treatment of polluted aqueous solutions by Ni^{2+}, Pb^{2+}, Zn^{2+}, Cr^{+6}, Cd^{+2} and Co^{+2} ions by ion exchange process using faujasite zeolite. *Procedia Engineering*, *33*(2011), 52–57. https://doi.org/10.1016/j.proeng.2012.01.1176

Mobasherpour, I., Salahi, E., & Pazouki, M. (2012). Comparative of the removal of Pb^{2+}, Cd 2+ and Ni 2+ by nano crystallite hydroxyapatite from aqueous solutions: Adsorption isotherm study. *Arabian Journal of Chemistry*, *5*(4), 439–446. https://doi.org/10.1016/j.arabjc.2010.12.022

Panda, D., Saini, C., Kumar, E. A., & Singh, S. K. (2020). In situ casting of rice husk ash in metal organic frameworks induces enhanced CO_2 capture performance. *Scientific Reports*, *10*(1). https://doi.org/10.1038/s41598-020-77213-9

Pourebrahimi, S., Kazemeini, M., & Vafajoo, L. (2017). Embedding graphene nanoplates into MIL-101(Cr) pores: Synthesis, characterization, and CO_2 adsorption studies. *Industrial and Engineering Chemistry Research*, *56*(14), 3895–3904. https://doi.org/10.1021/acs.iecr.6b04538

Rego, R. M., Sriram, G., Ajeya, K. V., Jung, H. Y., Kurkuri, M. D., & Kigga, M. (2021). Cerium based UiO-66 MOF as a multipollutant adsorbent for universal water purification. *Journal of Hazardous Materials*, *416*, 125941. https://doi.org/10.1016/j.jhazmat.2021.125941

Shadmehr, J., Zeinali, S., & Tohidi, M. (2019). Synthesis of a chromium terephthalate metal organic framework and use as nanoporous adsorbent for removal of diazinon organophosphorus insecticide from aqueous media. *Journal of Dispersion Science and Technology*, *40*(10), 1423–1440. https://doi.org/10.1080/01932691.2018.1516149

Shahriyari Far, H., Hasanzadeh, M., Najafi, M., Masale Nezhad, T. R., & Rabbani, M. (2021). Efficient removal of Pb(II) and Co(II) ions from aqueous solution with a chromium-based metal-organic framework/activated carbon composites. *Industrial and Engineering Chemistry Research*, *60*(11), 4332–4341. https://doi.org/10.1021/acs.iecr.0c06199

Sheikh Alivand, M., Hossein Tehrani, N. H. M., Shafiei-Alavijeh, M., Rashidi, A., Kooti, M., Pourreza, A., & Fakhraie, S. (2019). Synthesis of a modified HF-free MIL-101(Cr) nanoadsorbent with enhanced H_2S/CH_4 , CO_2 /CH_4, and CO_2 /N_2 selectivity. *Journal of Environmental Chemical Engineering*, *7*(2). https://doi.org/10.1016/j.jece.2019.102946

Tian, N., Jia, Q. M., Su, H. Y., Zhi, Y. F., Ma, A. H., Wu, J., & Shan, S. Y. (2016). The synthesis of mesostructured NH2-MIL-101(Cr) and kinetic and thermodynamic study in tetracycline aqueous solutions. *Journal of Porous Materials*, *23*(5), 1269–1278. https://doi.org/10.1007/s10934-016-0186-z

Trung, T. K., Ramsahye, N. A., Trens, P., Tanchoux, N., Serre, C., Fajula, F., & Férey, G. (2010). Adsorption of C5-C9 hydrocarbons in microporous MOFs MIL-100(Cr) and MIL-101(Cr): A manometric study. *Microporous and Mesoporous Materials*, *134*(1–3), 134–140. https://doi.org/10.1016/j.micromeso.2010.05.018

Vo, T. K., Kim, W. S., & Kim, J. (2020). Ethylenediamine-incorporated MIL-101(Cr)-NH_2 metal-organic frameworks for enhanced CO_2 adsorption. *Korean Journal of Chemical Engineering*, *37*(7), 1206–1211. https://doi.org/10.1007/s11814-020-0548-8

Wang, S., Xu, Y., Norbu, N., & Wang, Z. (2018). Remediation of biochar on heavy metal polluted soils. *IOP Conf. Ser.: Earth Environ. Sci. 108*, *108*(042113). https://doi.org/10.1088/1755-1315/108/4/042113

Wang, T., Zhao, P., Lu, N., Chen, H., Zhang, C., & Hou, X. (2016). Facile fabrication of Fe_3O_4/MIL-101(Cr) for effective removal of acid red 1 and orange G from aqueous solution. *Chemical Engineering Journal*, *295*, 403–413. https://doi.org/10.1016/j.cej.2016.03.016

Wu, J., Zhou, J., Zhang, S., Alsaedi, A., Hayat, T., Li, J., & Song, Y. (2019). Efficient removal of metal contaminants by EDTA modified MOF from aqueous solutions. *Journal of Colloid and Interface Science*, *555*, 403–412. https://doi.org/10.1016/j.jcis.2019.07.108

Zhang, F., Hao, L., Zhang, L., & Zhang, X. (2011). Solid-state thermolysis preparation of Co_3O_4

nano/micro superstructures from metal-organic framework for supercapacitors. *International Journal of Electrochemical Science*, *6*(7), 2943–2954. https://doi.org/10.1016/s1452-3981(23)18230-7

Zhang, J. Y., Zhang, N., Zhang, L., Fang, Y., Deng, W., Yu, M., Wang, Z., Li, L., Liu, X., & Li, J. (2015). Adsorption of uranyl ions on amine-functionalization of mil-101(cr) nanoparticles by a facile coordination-based post-synthetic strategy and x-ray absorption spectroscopy studies. *Scientific Reports*, *5*(October). https://doi.org/10.1038/srep13514

Zhao, T., Yang, L., Feng, P., Gruber, I., Janiak, C., & Liu, Y. (2018). Facile synthesis of nano-sized MIL-101(Cr) with the addition of acetic acid. *Inorganica Chimica Acta*, *471*, 440–445. https://doi.org/10.1016/j.ica.2017.11.030

Zhong, R., Yu, X., Meng, W., Liu, J., Zhi, C., & Zou, R. (2018). Amine-grafted MIL-101(Cr) via double-solvent incorporation for synergistic enhancement of CO2 uptake and selectivity. *ACS Sustainable Chemistry and Engineering*, *6*(12), 16493–16502. https://doi.org/10.1021/acssuschemeng.8b03597

Zhu, H., Yuan, J., Tan, X., Zhang, W., Fang, M., & Wang, X. (2019). Efficient removal of Pb 2+ by Tb-MOFs: identifying the adsorption mechanism through experimental and theoretical investigations. *Environmental Science: Nano*, *6*(1), 261–272. https://doi.org/10.1039/c8en01066h

Zou, M., Dong, M., & Zhao, T. (2022). Advances in metal-organic frameworks MIL-101(Cr). In *International Journal of Molecular Sciences* (Vol. 23, Issue 16). https://doi.org/10.3390/ijms23169396